Research Article

Towards growth of pure AB-stacked bilayer graphene single crystals

Xiaowen Zhang[1,2,3,§], Tao Zhou[1,2,§], Yunlong Ren[1,2,§], Zuo Feng[4,§], Ruixi Qiao[5], Qinghe Wang[4], Bin Wang[1,2], Jinxia Bai[1,2], Muhong Wu[4,6,7], Zhilie Tang[1,2], Xu Zhou[1,2], Kaihui Liu[4,6,7], and Xiaozhi Xu[1,2] (✉)

[1] Guangdong Basic Research Center of Excellence for Structure and Fundamental Interactions of Matter, Guangdong Provincial Key Laboratory of Quantum Engineering and Quantum Materials, School of Physics, South China Normal University, Guangzhou 510006, China

[2] Guangdong-Hong Kong Joint Laboratory of Quantum Matter, School of Physics, South China Normal University, Guangzhou 510006, China

[3] Physical Science and Engineering Division, King Abdullah University of Science and Technology, Thuwal 23955–6900, Saudi Arabia

[4] State Key Laboratory for Mesoscopic Physics, Frontiers Science Center for Nano-optoelectronics, School of Physics, Peking University, Beijing 100871, China

[5] Institute for Frontier Science, Nanjing University of Aeronautics and Astronautics, Nanjing 210094, China

[6] International Centre for Quantum Materials, Collaborative Innovation Centre of Quantum Matter, Peking University, Beijing 100871, China

[7] Songshan Lake Materials Laboratory, Institute of Physics, Chinese Academy of Sciences, Dongguan 523808, China

§ Xiaowen Zhang, Tao Zhou, Yunlong Ren, and Zuo Feng contributed equally to this work.

ABSTRACT

Given its intriguing band structure and unique tunable bandgap, AB-stacked bilayer graphene has great potentials in the applications of high-end electronics, optoelectronics and semiconductors. The epitaxial growth of AB-stacked single-crystal bilayer graphene films requires a strict AB-stacked lattice, identical orientations and seamless stitching of bilayer graphene islands. However, the particles inevitably present on the metal surface that produced during high temperature growth would induce random orientations, twisted stacking islands, and uncontrollable multilayers, which is a great challenge to overcome. Here, we propose a heat-resisting-box assisted strategy to produce nearly pure AB-stacked bilayer graphene single-crystal films on Cu/Ni (111) foils. With our technique, the particles on the Cu/Ni (111) surface are effectively eliminated, which greatly minimizes the occurrence of randomly twisted islands and uncontrollable multilayers. The as-grown AB-stacked bilayer graphene films show > 99% alignment and > 99% AB stacking order. Our work provides a promising method towards the growth of pure AB-stacked bilayer graphene single crystals and would accelerate its device applications.

KEYWORDS

bilayer graphene, AB stacking, uniform growth, heat-resisting box

1 Introduction

The tunable bandgap in graphene offers exciting potential applications in nanoelectronics [1–5]. In contrast to the monolayer graphene with zero bandgap, AB-stacked bilayer graphene exhibits a parabolic energy band structure owing to the interlayer π-orbitals coupling [6]. This unique configuration allows for the generation of a potential displacement field between graphene layers by applying an external vertical electric field, thereby enabling a bandgap up to 0.25 eV [7]. The bandgap can also be tuned by the applied electric field, strain and molecular doping [8–11]. Recently, some novel quantum states including topological energy valley transport [12], tunable excitons [13], giant valley selective Hall effect [14] and fractional quantum Hall states [15] in AB-stacked bilayer graphene have been observed. In addition to the interesting physical phenomena, it also presents a vast array of opportunities for electronics and photonics, ranging from field effect transistors, photodetectors, modulators to topological quantum computing [16–19]. As such, the scalable production of highly crystalline bilayer graphene with a precisely controlled AB-stacked structure holds paramount significance for both fundamental researches and those prospective applications.

Over the past decade, extensive efforts have been employed on the controllable growth of AB-stacked bilayer graphene single crystals [20–25]. Initially, early attempts were focused on the growth on Cu (111) foils due to its well-established mature and extensive growth process [26–29]. However, this approach was plagued by a "self-limited" growth behaviour, where the growth of the second layer was impeded once the first layer fully covered the Cu surface. Although some methods such as the spatial arrangement of Cu foils [30], high H_2/CH_4 ratio [31, 32], special Cu enclosures [33], or the employment of O-rich Cu foils were tried [34], the controlled growth of bilayer graphene films remains to be improved. Subsequently, researchers found that using Cu-Ni or Cu-Si alloy substrates was a better choice and the growth of bilayer graphene single crystal has been partially realized [20, 21], where the solubility of carbon atoms can be finely modulated through alloying. Nevertheless, despite these developments, several hurdles are still waiting to be found and overcome. As previously reported, the high temperature will produce silica particles shedding from the quartz tube during growth [35–37], which may act as nucleation sites and result in random orientations and multilayer areas that often observed in the actual chemical vapor

deposition (CVD) growth. Therefore, there are still ample room for further exploration and advancement in the production of pure AB-stacked bilayer graphene single crystals.
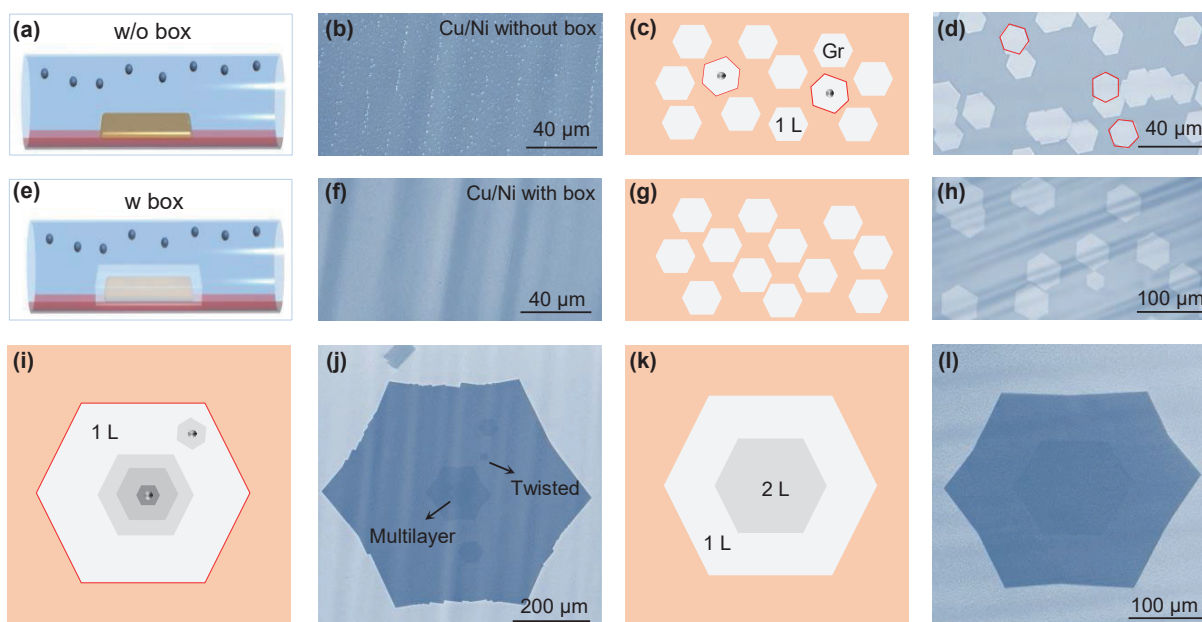
In this work, we used a simple heat-resisting box technique to ideally avoid particle contamination on the metal surface to prepare almost pure AB-stacked bilayer graphene single-crystal films on Cu/Ni (111) foils. With our technique, almost all of the particles on the Cu/Ni (111) surface were effectively eliminated, thus significantly reducing the random orientations and uncontrollable multilayers. Systematic analysis demonstrated that compared with the Cu/Ni (111) without treatment, the treated substrates showed significant improvement in the alignment of monolayer graphene, AB-stacking ratio and the uniformity of bilayer graphene films. The grown AB-stacked bilayer graphene films show > 99% alignment and < 1% multilayer areas. Our work addresses an often-overlooked problem in the production of AB-stacked single-crystal bilayer graphene and is expected to advance their device applications.
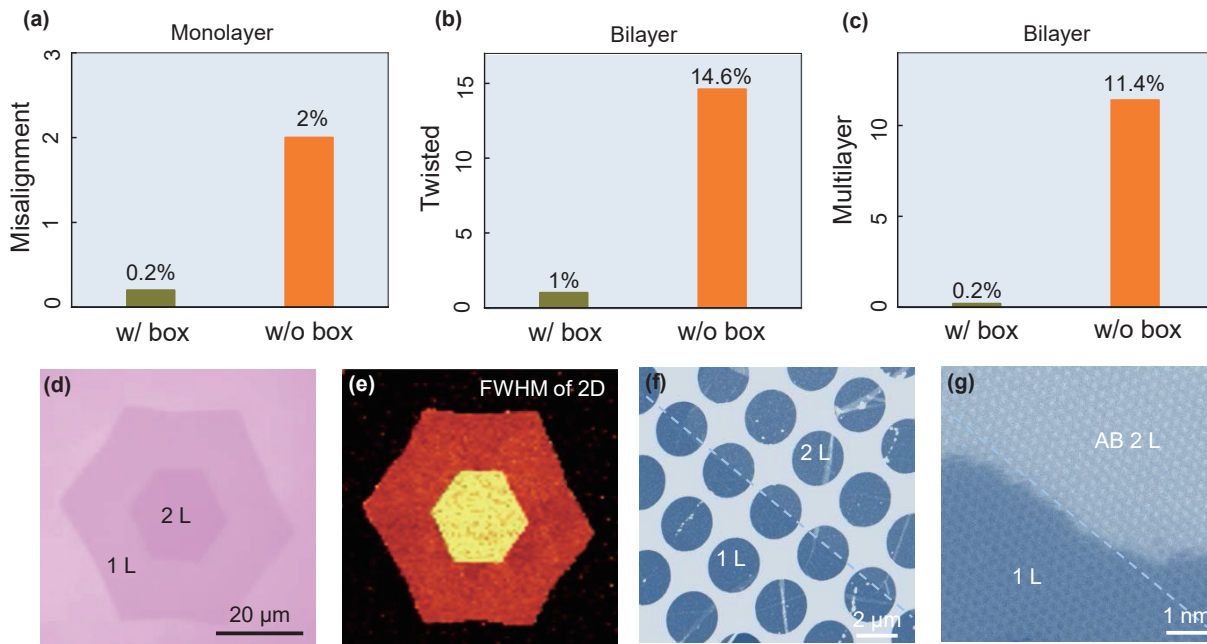
2   Results and discussion

In a conventional CVD system, Cu/Ni foils are usually directly exposed to the atmosphere throughout the growth process and some small particles are always observed on the Cu/Ni surface (Figs. 1(a) and 1(b)), which were demonstrated to be silica particles from the quartz tube during the CVD process (Fig. S1 in the Electronic Supplementary Material (ESM)) [38]. Such particles are very difficult to remove once deposited on the substrate, and they would serve as "undesirable" nucleation sites during graphene growth and induce islands with uncontrollable orientations (Figs. 1(c) and 1(d)). That is why misaligned graphene islands are frequently observed in CVD-grown graphene, even on a lattice-matched Cu (111) substrate [39]. By further characterizations of the as-grown monolayer graphene on Cu/Ni (111) foils, we found that the misaligned graphene islands are randomly oriented, which would inevitably affect the aligned growth of the second layer graphene. In order to solve this

problem, we introduced a home-designed heat-resisting box into the CVD system (the box is made of graphite and is rectangular in shape. There are several small holes on the side to allow air flow in, the optical image of the box is shown in Fig. S2 in the ESM), which has been used to grow graphene with low dot defects [38]. The Cu/Ni foil was placed in the box and loaded into the CVD system, which prevented the released silica particles in the atmosphere from deposition on the surface (Fig. 1(e)). Then a clean and uniform Cu/Ni (111) surface can be obtained after annealing (Fig. 1(f) and Fig. S3 in the ESM), followed by the direct growth of high-quality graphene. Without the influence of particles on the surface, all the graphene islands trend to grow with the same orientation that dominated by the van der Waals interaction (Figs. 1(g) and 1(h)) [39, 40]. To grow AB-stacked bilayer graphene, we need the strict epitaxy of the second layer graphene. However, the silica particles existing in conventional CVD system would also act as nucleation sites for the second layer graphene, thus inducing multilayer areas and uncontrollable twisted stacking (Figs. 1(i) and 1(j) and Fig. S4 in the ESM). With our design, the particles are avoided and most of the second layer graphene are grown with AB stacking as this configuration is most energetically favourable [41]. Better yet, the multilayer areas can also be greatly reduced as the particles that act as multilayer nucleation sites disappear (Figs. 1(k) and 1(l)).

Further improving the alignment of the first layer graphene and AB stacking ratio of the second layer graphene lays a foundation for the production of nearly pure AB-stacked bilayer graphene single crystals. And the elimination of multilayer regions ensures the uniformity of the sample. We performed statistical analysis of more than 1000 bilayer graphene islands with and without the heat-resisting boxes (typical optical images are shown in Fig. S5 in the ESM). The statistical distribution of misalignment of monolayer graphene grown with and without box is shown in Fig. 2(a). The misalignment percentage of monolayer graphene grown without box is about 2%, while changing to 0.2% with our design, about 10 times decreasing. For bilayer graphene growth, the ratios of twisted bilayer graphene and multilayers are up to

Figure 1 Designed growth of AB-stacked bilayer graphene. (a) Schematic diagram of a conventional CVD growth system of graphene on Cu/Ni (111) foil. (b) Representative SEM image of annealed Cu/Ni (111) surface directly placed in a quartz tube. Many particles can be found. (c) Schematic diagram and (d) optical image of monolayer graphene grown by conventional CVD method. Twisted domains are marked with dashed red hexagons. (e) Schematic diagram of a designed CVD growth system with a heat-resisting box. (f) Representative SEM image of annealed Cu/Ni (111) surface. No particles can be observed. (g) Schematic diagram and (h) optical image of monolayer graphene grown with the box. (i) Schematic diagram and (j) optical image of bilayer graphene grown by conventional CVD method. Twisted and multilayer islands can be found. (k) Schematic diagram and (l) optical image of bilayer graphene grown with the box, and only uniform bilayer graphene exists.
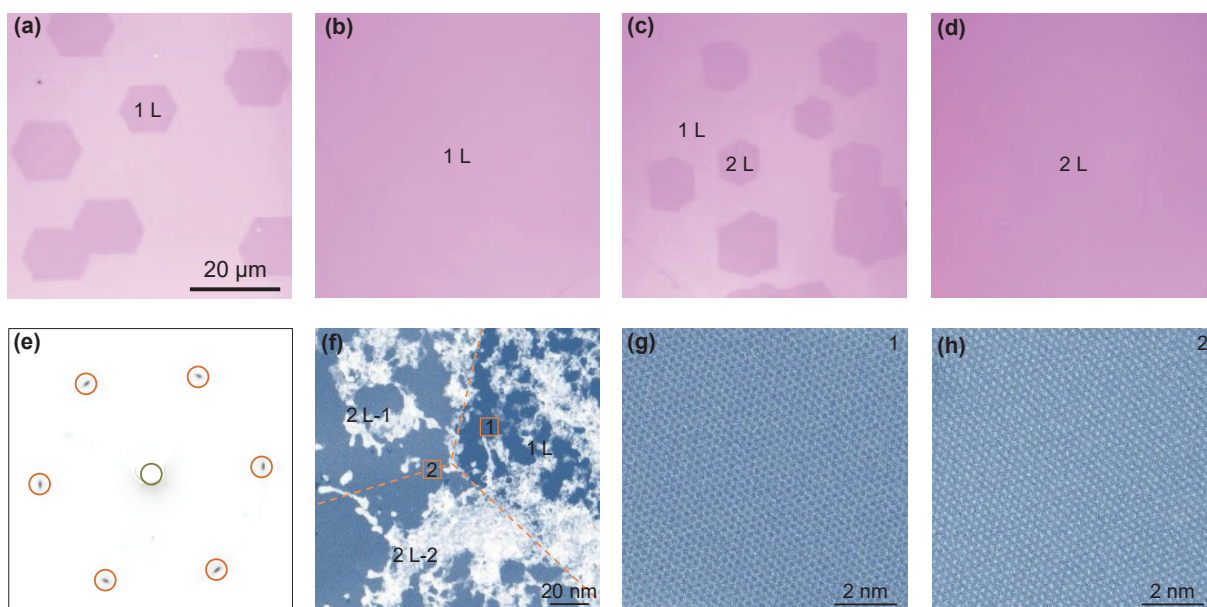
Figure 2 Statistical data and characterizations of as-grown bilayer graphene with and without heat-resisting box. (a)–(c) Statistical distributions of misalignment in monolayer (a), twisted (b) and multilayer regions (c) in bilayer graphene grown with and without heat-resisting box. (d) Optical image and (e) the corresponding FWHM mapping of 2D band of an as-grown AB-stacked bilayer graphene island. (f) and (g) TEM images of the edge area of monolayer and bilayer graphene samples.

14.6% and 11.4% in conventionally growth, but decrease to 1% and 0.2% when growing with box (Figs. 2(b) and 2(c)). These data demonstrate that the epitaxy of uniform AB-stacked bilayer graphene has been greatly improved.

Subsequently, we verified the AB stacking structure and high quality of the as-grown bilayer graphene samples by spectroscopic and atomic-resolved transmission electron microscopy (TEM) characterizations. For the Raman spectra, the intensity ratio of 2D/G is about 1, the 2D band can be perfectly fitted by four Lorentz curves, the full-width at half maximum (FWHM) of 2D band and the four Lorentz curves are 54 and 31 cm^{-1}, respectively, all the data indicate that the samples are uniform AB-stacked bilayer graphene (Figs. 2(d) and 2(e), and Fig. S6 in the ESM). Further TEM images and selected area electron diffraction (SAED) patterns undoubtedly demonstrated the AB stacking

order at atomic scale directly in both real space and reciprocal space (Figs. 2(f) and 2(g), and Fig. S7 in the ESM).

So far, we have shown that the uniform AB-stacked bilayer graphene islands can be achieved by removing the silica particles on the Cu/Ni (111) surface. Then, we further validated our design on the production of AB-stacked bilayer graphene single crystals by the seamless stitching of both monolayer and bilayer graphene islands. By increasing the growth time, we can successively obtain aligned monolayer graphene islands (Fig. 3(a)), single-crystal monolayer graphene films (Fig. 3(b)), bilayer graphene islands (Fig. 3(c)), and single-crystal bilayer graphene films (Fig. 3(d)). The high coverage of bilayer graphene on the Cu/Ni (111) substrate is primarily facilitated by the segregation, rather than surface-mediated growth, which is attributed to the optimal Cu/Ni ratio [20]. The stacking order and lattice orientations over large

Figure 3 Growth and seamless stitching of single-crystal bilayer graphene films. (a)–(d) Optical images showing the time evolution of AB-stacked bilayer graphene samples transferred onto SiO₂/Si substrates. (e) A typical LEED pattern of the as-grown bilayer graphene. (f) Low-magnification TEM image of a merged area of two bilayer graphene islands. The white floc-like deposition on graphene is the residual PMMA during the wet transfer of samples onto TEM grids. Atomically-resolved TEM images of the (g) monolayer (marked as 1 in (f)) and (h) bilayer (marked as 2 in (f)) regions of graphene, no grain boundary was found.

area were verified by low energy electron diffraction (LEED) characterizations. The LEED patterns show nearly identical orientations throughout the samples, indicating perfect alignment of the graphene lattice. Only one set of hexagonal diffraction spots in the LEED patterns also once again demonstrate the AB stacking order (Fig. 3(e) and Fig. S8 in the ESM), as twisted bilayer graphene will produce two sets of hexagonal diffraction spots [42]. The seamless stitching of the bilayer graphene islands was checked by TEM characterizations at the merged region. The atomic-resolved TEM images clearly show the seamless stitching of two neighbouring bilayer graphene islands (Figs. 3(f)–3(h)). With our design, we have successfully produced 4 cm × 4 cm uniform AB-stacked single-crystal bilayer graphene films (Fig. S9 in the ESM).

The quality of the samples was first checked by Raman spectra. We extracted the data to show the statistical distributions of the FWHM of 2D band and the intensity ratio of 2D/G band of graphene (Fig. 4(a)). The highly concentrated distribution proves the good homogeneity of the sample. Furthermore, we compared the quality of AB-stacked bilayer graphene samples obtained with and without the box, and found obvious improvement with our technique. Since the particles on the surface are removed, the graphene surface should be cleaner and more intact, so the quality of the sample should be higher. The field-effect transistors (FETs) were directly fabricated on 300 nm SiO_2/Si substrates (Fig. 4(b)) with a conventional process (see details in the Method section). The electrical measurements were conducted at room temperature and an averaged carrier mobility of 7348 $cm^2 \cdot V^{-1} \cdot s^{-1}$ was obtained for the sample grown with box. As a contrast, the carrier mobility of graphene grown without the box is just 5125 $cm^2 \cdot V^{-1} \cdot s^{-1}$, which may be attributed to the uncontrollable nano-particles on the substrate surface (Fig. 4(c)).

3   Conclusion

In summary, we proposed an effective strategy for achieving the epitaxial growth of bilayer graphene single crystals with highly aligned orientation and strict AB-stacking by eliminating substrate impurities on Cu/Ni (111) foils. We revealed that the inevitable particles on the surface would influence the growth of graphene and result in twisted islands and multilayers. By applying a designed heat-resistant box to prevent particles deposition on the substrate, we were able to successfully produce large-area AB-stacked bilayer single-crystal graphene films, of which the orientation consistency and AB stacking sequence show more than 99%. The high crystalline quality and uniformity of the as-grown film were confirmed through Raman spectroscopy, TEM and electrical measurements. Our work provides a simple method towards the growth of pure AB-stacked bilayer graphene single crystals and would accelerate its device applications.
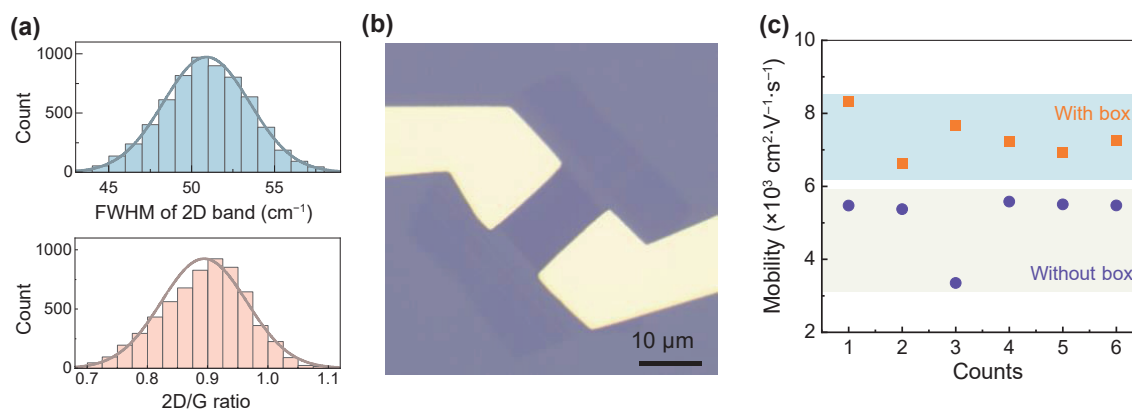
4   Method

Preparation of Cu/Ni (111) foils: 25 μm thick Cu (111) foils were prepared by high-temperature annealing (~ 1050 °C) of commercial Cu foils (25 μm thick, 99.8%, Sichuan Oriental Stars Trading Co. Ltd) under an Ar/H_2 flow at atmospheric pressure. A nickel layer was plated on both sides of the Cu (111) foil in an electrolyte, which was prepared by dissolving 70 g of $NiSO_4 \cdot 6H_2O$, 2 g of $NiCl_2 \cdot 6H_2O$, 1 g of NaF and 7.5 g of H_3BO_3 in 250 mL deionized water. The applied current density was 0.02 $A \cdot cm^{-2}$. After washing and drying, the Ni-plated Cu (111) foil was annealed in a CVD system at 1050 °C for 5 h to obtain the Cu/Ni (111) foil. The optimal Ni concentration is 14 at.% in our experiment, which gives the best uniformity and coverage of bilayer graphene (Fig. S10 in the ESM).

Growth of bilayer graphene on Cu/Ni (111) foils: The Cu/Ni (111) foils were placed in a heat-resisting box and then directly loaded into a CVD furnace (Tianjin Kaiheng). The system was heated to 1100 °C in 1 h with Ar (500 sccm) followed by annealing in additional H_2 (30 sccm) for 40 min. Then CH_4 (4.0 sccm) was introduced as the carbon source for graphene growth for different time (the growth behaviours at different temperature and H_2/CH_4 ratio can be seen in Fig. S11 in the ESM). Finally, the sample was rapidly cooled down to room temperature by moving the heat-resisting box to the upstream side of the CVD chamber under a constant H_2/Ar flow.

Characterization: LEED measurements were performed using Omicron LEED system in ultra high vacuum (UHV). Scanning electron microscopy (SEM) images were obtained using a Thermal Fisher Quattro S Environmental SEM. The graphene sample for TEM characterization was prepared by transferring graphene onto commercial holey-carbon TEM grids (Zhongjingkeyi GIG-2010-3C) using the polymethyl methacrylate (PMMA) transfer technique. Scanning TEM (STEM) and SAED experiments were performed in an FEI Titan Themis G2 300 instrument operated at 300 kV. Optical images were conducted with an Olympus microscope (Olympus BX51). Raman spectra and mappings were obtained with an alpha300R system (WITec, Germany) with a laser excitation wavelength of 532 nm.

Device fabrications and measurements: The FETs were fabricated through standard microfabrication process by electron beam lithography techniques. The Cr/Au contact electrodes (~ 5/50 nm) were fabricated by e-beam deposition system with a low vacuum ~ 3 × 10^{-7} Pa. All the electrical measurements were

Figure 4   The quality characterizations of as-grown AB-stacked bilayer graphene. (a) Statistical distributions of the FWHM of 2D band (upper panel) and intensity ratio of 2D/G band (lower panel) of graphene in large area. (b) Optical image of an FET device. (c) Carrier mobility of graphene grown with and without heat-resisting box at room temperature.

carried out in a probe station (base pressure 10^{-4} Pa) with Agilent semiconductor parameter analyzer (B1500, high resolution modules) at room temperature.

Acknowledgements

Electronic Supplementary Material: Supplementary material (EDS measurements, photographs of the graphite box and bilayer graphene transferred onto a SiO_2/Si substrate, optical images of foils surface and twist bilayer graphene, statistical optical image of misalignment regions in bilayer graphene, Raman spectra, SAED pattern and LEED patterns of the bilayer graphene samples, optical images of graphene with different Cu/Ni ratio, temperature and H_2/CH_4 ratio) is available in the online version of this article at https://doi.org/10.1007/s12274-023-6348-9.

References

[1] Lin, L.; Deng, B.; Sun, J. Y.; Peng, H. L.; Liu, Z. F. Bridging the gap between reality and ideal in chemical vapor deposition growth of graphene. *Chem. Rev.* **2018**, *118*, 9281–9343.

[2] Xia, F. N.; Farmer, D. B.; Lin, Y. M.; Avouris, P. Graphene field-effect transistors with high on/off current ratio and large transport band gap at room temperature. *Nano Lett.* **2010**, *10*, 715–718.

[3] Chen, Y. C.; Cao, T.; Chen, C.; Pedramrazi, Z.; Haberer, D.; De Oteyza, D. G.; Fischer, F. R.; Louie, S. G.; Crommie, M. F. Molecular bandgap engineering of bottom-up synthesized graphene nanoribbon heterojunctions. *Nat. Nanotechnol.* **2015**, *10*, 156–160.

[4] Xu, X. Z.; Liu, C.; Sun, Z. H.; Cao, T.; Zhang, Z. H.; Wang, E. G.; Liu, Z. F.; Liu, K. H. Interfacial engineering in graphene bandgap. *Chem. Soc. Rev.* **2018**, *47*, 3059–3099.

[5] Zhou, S. Y.; Gweon, G. H.; Fedorov, A. V.; First, P. N.; De Heer, W. A.; Lee, D. H.; Guinea, F.; Neto, A. H. C.; Lanzara, A. Substrate-induced bandgap opening in epitaxial graphene. *Nat. Mater.* **2007**, *6*, 770–775.

[6] Chen, Z. L.; Qi, Y.; Chen, X. D.; Zhang, Y. F.; Liu, Z. F. Direct CVD growth of graphene on traditional glass: Methods and mechanisms. *Adv. Mater.* **2019**, *31*, 1803639.

[7] Zhang, Y. B.; Tang, T. T.; Girit, C.; Hao, Z.; Martin, M. C.; Zettl, A.; Crommie, M. F.; Shen, Y. R.; Wang, F. Direct observation of a widely tunable bandgap in bilayer graphene. *Nature* **2009**, *459*, 820–823.

[8] Choi, S. M.; Jhi, S. H.; Son, Y. W. Controlling energy gap of bilayer graphene by strain. *Nano Lett.* **2010**, *10*, 3486–3489.

[9] Verberck, B.; Partoens, B.; Peeters, F. M.; Trauzettel, B. Strain-induced band gaps in bilayer graphene. *Phys. Rev. B* **2012**, *85*, 125403.

[10] Zhang, W. J.; Lin, C. T.; Liu, K. K.; Tite, T.; Su, C. Y.; Chang, C. H.; Lee, Y. H.; Chu, C. W.; Wei, K. H.; Kuo, J. L. et al. Opening an electrical band gap of bilayer graphene with molecular doping. *ACS Nano,* **2011**, *5*, 7517–7524.

[11] Mak, K. F.; Lui, C. H.; Shan, J.; Heinz, T. F. Observation of an electric-field-induced band gap in bilayer graphene by infrared spectroscopy. *Phys. Rev. Lett.* **2009**, *102*, 256405.

[12] Ju, L.; Shi, Z. W.; Nair, N.; Lv, Y. C.; Jin, C. H.; Velasco, J.; Ojeda-Aristizabal, C.; Bechtel, H. A.; Martin, M. C.; Zettl, A. et al. Topological valley transport at bilayer graphene domain walls. *Nature* **2015**, *520*, 650–655.

[13] Ju, L.; Wang, L.; Cao, T.; Taniguchi, T.; Watanabe, K.; Louie, S. G.; Rana, F.; Park, J.; Hone, J.; Wang, F. et al. Tunable excitons in bilayer graphene. *Science* **2017**, *358*, 907–910.

[14] Yin, J. B.; Tan, C.; Barcons-Ruiz, D.; Torre, I.; Watanabe, K.; Taniguchi, T.; Song, J. C. W.; Hone, J.; Koppens, F. H. L. Tunable and giant valley-selective Hall effect in gapped bilayer graphene. *Science* **2022**, *375*, 1398–1402.

[15] Li, J. I. A.; Tan, C.; Chen, S.; Zeng, Y.; Taniguchi, T.; Watanabe, K.; Hone, J.; Dean, C. R. Even-denominator fractional quantum Hall states in bilayer graphene. *Science* **2017**, *358*, 648–652.

[16] Szafranek, B. N.; Schall, D.; Otto, M.; Neumaier, D.; Kurz, H. High on/off ratios in bilayer graphene field effect transistors realized by surface dopants. *Nano Lett.* **2011**, *11*, 2640–2643.

[17] Jung, M.; Rickhaus, P.; Zihlmann, S.; Makk, P.; Schönenberger, C. Microwave photodetection in an ultraclean suspended bilayer graphene p-n junction. *Nano Lett.* **2016**, *16*, 6988–6993.

[18] Wu, S. F.; Mao, L.; Jones, A. M.; Yao, W.; Zhang, C. W.; Xu, X. D. Quantum-enhanced tunable second-order optical nonlinearity in bilayer graphene. *Nano Lett.* **2012**, *12*, 2032–2036.

[19] Liu, X. L.; Hersam, M. C. 2D materials for quantum information science. *Nat. Rev. Mater.* **2019**, *4*, 669–684.

[20] Huang, M.; Bakharev, P. V.; Wang, Z. J.; Biswal, M.; Yang, Z.; Jin, S.; Wang, B.; Park, H. J.; Li, Y. Q.; Qu, D. S. et al. Large-area single-crystal AB-bilayer and ABA-trilayer graphene grown on a Cu/Ni(III) foil. *Nat. Nanotechnol.* **2020**, *15*, 289–295.

[21] Nguyen, V. L.; Duong, D. L.; Lee, S. H.; Avila, J.; Han, G.; Kim, Y. M.; Asensio, M. C.; Jeong, S. Y.; Lee, Y. H. Layer-controlled single-crystalline graphene film with stacking order via Cu-Si alloy formation. *Nat. Nanotechnol.* **2020**, *15*, 861–867.

[22] Liu, W.; Kraemer, S.; Sarkar, D.; Li, H.; Ajayan, P. M.; Banerjee, K. Controllable and rapid synthesis of high-quality and large-area bernal stacked bilayer graphene using chemical vapor deposition. *Chem. Mater.* **2014**, *26*, 907–915.

[23] Gao, Z. L.; Zhang, Q. C.; Naylor, C. H.; Kim, Y.; Abidi, I. H.; Ping, J. L.; Ducos, P.; Zauberman, J.; Zhao, M. Q.; Rappe, A. M. et al. Crystalline bilayer graphene with preferential stacking from Ni-Cu gradient alloy. *ACS Nano* **2018**, *12*, 2275–2282.

[24] Qian, Y. T.; Kang, D. J. Large-area high-quality AB-stacked bilayer graphene on h-BN/Pt foil by chemical vapor deposition. *ACS Appl. Mater. Interfaces* **2018**, *10*, 29069–29075.

[25] Deng, B.; Liu, Z. F.; Peng, H. L. Toward mass production of CVD graphene films. *Adv. Mater.* **2019**, *31*, 1800996.

[26] Gao, L. B.; Ni, G. X.; Liu, Y. P.; Liu, B.; Neto, A. H. C.; Loh, K. P. Face-to-face transfer of wafer-scale graphene films. *Nature* **2014**, *505*, 190–194.

[27] Gao, L. B.; Ren, W. C.; Xu, H. L.; Jin, L.; Wang, Z. X.; Ma, T.; Ma, L. P.; Zhang, Z. Y.; Fu, Q.; Peng, L. M. et al. Repeated growth and bubbling transfer of graphene with millimetre-size single-crystal grains using platinum. *Nat. Commun.* **2012**, *3*, 699.

[28] Reina, A.; Jia, X. T.; Ho, J.; Nezich, D.; Son, H.; Bulovic, V.; Dresselhaus, M. S.; Kong, J. Large area, few-layer graphene films on arbitrary substrates by chemical vapor deposition. *Nano Lett.* **2009**, *9*, 30–35.

[29] Zhang, J. C.; Liu, X. T.; Zhang, M. Q.; Zhang, R.; Ta, H. Q.; Sun, J. B.; Wang, W. D.; Zhu, W. Q.; Fang, T. T.; Jia, K. C. et al. Fast synthesis of large-area bilayer graphene film on Cu. *Nat. Commun.* **2023**, *14*, 3199.

[30] Yan, K.; Peng, H. L.; Zhou, Y.; Li, H.; Liu, Z. F. Formation of bilayer bernal graphene: Layer-by-layer epitaxy via chemical vapor deposition. *Nano Lett.* **2011**, *11*, 1106–1110.

[31] Liu, L. X.; Zhou, H. L.; Cheng, R.; Yu, W. J.; Liu, Y.; Chen, Y.; Shaw, J.; Zhong, X.; Huang, Y.; Duan, X. F. High-yield chemical vapor deposition growth of high-quality large-area AB-stacked bilayer graphene. *ACS Nano* **2012**, *6*, 8241–8249.

[32] Ta, H. Q.; Perello, D. J.; Duong, D. L.; Han, G. H.; Gorantla, S.; Nguyen, V. L.; Bachmatiuk, A.; Rotkin, S. V.; Lee, Y. H.; Rümmeli,

M. H. Stranski-krastanov and volmer-weber CVD growth regimes to control the stacking order in bilayer graphene. *Nano Lett.* **2016**, *16*, 6403–6410.

[33] Fang, W. J.; Hsu, A. L.; Song, Y.; Birdwell, A. G.; Amani, M.; Dubey, M.; Dresselhaus, M. S.; Palacios, T.; Kong, J. Asymmetric growth of bilayer graphene on copper enclosures using low-pressure chemical vapor deposition. *ACS Nano,* **2014**, *8*, 6491–6499.

[34] Hao, Y. F.; Wang, L.; Liu, Y. Y.; Chen, H.; Wang, X. H.; Tan, C.; Nie, S.; Suk, J. W.; Jiang, T. F.; Liang, T. F. et al. Oxygen-activated growth and bandgap tunability of large single-crystal bilayer graphene. *Nat. Nanotechnol.* **2016**, *11*, 426–431.

[35] Jiang, B.; Liang, D. D.; Sun, Z. T.; Ci, H.; Liu, B. Z.; Gao, Y. Q.; Shan, J. Y.; Yang, X. Q.; Rümmeli, M. H.; Wang, J. X. et al. Toward direct growth of ultra‑flat graphene. *Adv. Funct. Mater.* **2022**, *32*, 2200428.

[36] Ge, X. M.; Zhang, Y. H.; Chen, L. X.; Zheng, Y. H.; Chen, Z. Y.; Liang, Y. J.; Hu, S. K.; Li, J.; Sui, Y.; Yu, G. H. et al. Mechanism of SiO_x particles formation during CVD graphene growth on Cu substrates. *Carbon* **2018**, *139*, 989–998.

[37] Wang, Z. J.; Weinberg, G.; Zhang, Q.; Lunkenbein, T.; Klein-Hoffmann, A.; Kurnatowska, M.; Plodinec, M.; Li, Q.; Chi, L. F.; Schloegl, R. et al. Direct observation of graphene growth and associated copper substrate dynamics by *in situ* scanning electron microscopy. *ACS Nano* **2015**, *9*, 1506–1519.

[38] Xu, X. Z.; Qiao, R. X.; Liang, Z. H.; Zhang, R.; Zeng, F. K.; Cui, G. L.; Zhang, X. W.; Zou, D. X.; Guo, Y.; Liu, C. et al. Towards intrinsically pure graphene grown on copper. *Nano Res.* **2022**, *15*, 919–924.

[39] Nguyen, V. L.; Shin, B. G.; Duong, D. L.; Kim, S. T.; Perello, D.; Lim, Y. J.; Yuan, Q. H.; Ding, F.; Jeong, H. Y.; Shin, H. S. et al. Seamless stitching of graphene domains on polished copper (111) foil. *Adv. Mater.* **2015**, *27*, 1376–1382.

[40] Xu, X. Z.; Zhang, Z. H.; Dong, J. C.; Yi, D.; Niu, J. J.; Wu, M. H.; Lin, L.; Yin, R. K.; Li, M. Q.; Zhou, J. Y. et al. Ultrafast epitaxial growth of metre-sized single-crystal graphene on industrial Cu foil. *Sci. Bull.* **2017**, *62*, 1074–1080.

[41] Sun, L. Z.; Wang, Z. H.; Wang, Y. C.; Zhao, L.; Li, Y. L. Z.; Chen, B. H.; Huang, S. H.; Zhang, S. S.; Wang, W. D.; Pei, D. et al. Hetero-site nucleation for growing twisted bilayer graphene with a wide range of twist angles. *Nat. Commun.* **2021**, *12*, 2391.

[42] Wei, W.; Zhang, C.; Li, H. B.; Pan, J. Q.; Tan, Z.; Li, Y. J.; Cui, Y. *In situ* growth dynamics of uniform bilayer graphene with different twisted angles following layer-by-layer mode. *J. Phys. Chem. Lett.* **2022**, *13*, 11201–11207.